VOCs Emission from a Final Landfill Cover System Induced by Ground Surface Air Temperature and Barometric Pressure Fluctuation

Qiao Wang [a], Haijian Xie [b, c]*, Yingfei Peng [b], Arif Mohammad [d], Devendra Narain Singh [e]

[a] School of Resource and Environmental Engineering, Hefei University of Technology, Hefei, 230009, China.

[b] College of Civil Engineering and Architecture, Zhejiang University, 866 Yuhangtang Rd., Hangzhou, 310058, China.

[c] Center for Balance Architecture, Zhejiang University, 148 Tianmushan Road, Hangzhou, 310007, China.

[d] School of Engineering, Cardiff University, Queen's Buildings, The Parade Cardiff CF24 3AA, UK.

[e] Department of Civil Engineering, Indian Institute of Technology Bombay, Mumbai, 400076, India.

*Corresponding author, Ph.D. Professor, College of Civil Engineering and Architecture, Zhejiang Univ. 866 Yuhangtang Rd. Hangzhou 310058, China.

E-mail: xiehaijian@zju.edu.cn

Abstract

Volatile organic compounds (VOCs) emission flux and their concentration profiles were measured at a final municipal solid waste (MSW) landfill cover in Hangzhou, China. The influencing parameters, especially ground surface air temperature and pressure were monitored concomitantly. Furthermore, a numerical model incorporating coupled thermo-hydro-chemical interaction to assess VOCs emission from this final landfill cover (LFC) system was developed and validated with the field test results. The tested total VOC emission flux from the final cover is 0.0124 $\mu g/m^2/s$, which indicates that the total amount of VOCs emitted into the atmosphere is 391 mg/m^2 annually. Among these, dichloromethane (DCM) dominated VOCs emission flux during May, comprising 51.8% of the total emission flux. The numerical simulation results indicated that the diffusive emission flux of VOCs varied consistently with the fluctuation of atmospheric temperature. Whereas, the advective flux varied inversely with the fluctuation of barometric pressure. The highest difference in diffusive emission flux induced by temperature variation is 183 $\mu g/m^2/day$ and occurred in spring. Moreover, the results demonstrated that the impact of atmospheric temperature and pressure fluctuation on the emission of VOC from final covers is non-negligible when reasonably assessing the risks of landfill and landfill gas emission budget.

Keywords: volatile organic compounds, landfill cover, emission flux, cover-atmosphere system, barometric pressure, ground surface air temperature

1 Introduction

Landfilling is adopted as an easy approach of MSW management and handling worldwide, despite having several threats to the environment due to the emission of gases and leachate (Mohammad et al., 2021, 2022; Yan et al., 2022; Hu et al., 2023). Degradation of manufactured and human-made products in MSW landfill will be a long-term source of VOCs to the surrounding environment (Wang et al., 2019). Landfill gas (LFG) emission can be mitigated by conventional engineering interventions such as LFG collection system (Barlaz et al., 2004) and landfill cover system (Xie et al., 2017, 2018; Wang et al., 2022). However, residual LFG, including VOCs that cannot be collected, degraded, and adsorbed, will be continuously emitted into the atmosphere for several decades (Zhan et al., 2015; Duan et al., 2021; Wang et al., 2022). Exposure to VOCs can cause various adverse health effects (Huang et al., 2014) as some VOCs are proven to be carcinogens, such as benzene (US EPA, 2009). Dichloromethane (DCM) was listed as the Key New Pollutants for Control (2022 edition) by the Ministry of Ecology and Environment of China (Mu et al., 2022).

VOCs can migrate through landfill cover systems by either advection or diffusion (Rowe et al., 2004), and then emitted into the atmosphere, leading to atmospheric transport (Lei et al., 2021). It is indicated by Massmann (1989) that advective flows induced by naturally occurring atmospheric pressure fluctuations are likely to enhance diffusive fluxes. The variation of atmospheric factors, including temperature and pressure, will lead to the fluctuation of landfill gas emissions (Kim and Benson, 2004; Xu et al., 2014; Shen et al., 2018; Ma et al., 2022; Kissas et al., 2023). This is because the diffusion and advection processes are substantially affected by the soil temperature and the pressure gradient (Feng et al., 2017a, b). It has been proven that seasonal fluctuation of ground surface temperature will induce the emission of tetrachloroethylene (PCE) and N_2O from groundwater (Ma et al., 2022) based on a coupled heat transfer and gas transport

model. The results indicate that both PCE and N_2O emissions fluctuated with the variation of ground surface temperature and lagged behind due to the damping effects of both capillary fringe and soil sorption. Based on the studies performed by Kissas et al. (2023) on the performance of a passive biocover system, it has been found that the methane oxidation efficiency patterns in LFC follow a similar trend of the rate of change in barometric pressure investigated.

Although landfill gas transport through cover barriers has been studied extensively (Hamamoto et al., 2011; Ng et al., 2015a; Xu et al., 2017; Xie et al., 2017, 2018, 2022; Feng et al., 2019), little attention has been paid on the atmospheric temperature and pressure fluctuation induced LFG emission, especially for VOCs. However, the behavior of LFG transport and the performance of the cover system interact closely with the changes of atmospheric factors (Ng et al., 2022). Atmospheric temperature and pressure fluctuation will induce the variation of soil temperature and gas pressure in soil, which will considerably impact LFG transport and emission into the atmosphere (Ma et al., 2022). This results in difficulty in evaluating the risks of landfill and LFG emission budget reasonably.

To bridge the gap, the primary objective of this study is to evaluate VOCs emission from a final LFC system that has been in service for 15 years considering the atmospheric variables, such as daily temperature and barometric pressure. The VOCs concentration profiles and emission flux were determined based on field tests at a MSW landfill in Hangzhou, China. The atmospheric factors including temperature, air relative humidity, wind speed and barometric pressure were obtained by real-time monitoring. A coupled effect of heat, moisture, and pressure on the mass transfer and emission of VOCs was investigated based on a numerical model. Pressure-induced advective emission and temperature-induced diffusive emission have been evaluated through

numerical simulation. This study provides new insight into the behaviour of contaminant transport in the cover-atmosphere system.

2 Materials and Methods

2.1 Site description

The test was conducted at the final cover system of a large-scale MSW landfill in Hangzhou, China (Figure 1a). The landfill was built in 1991 and closed in 2007 with a final cover system, composed of a 30 cm gravel layer for gas collection, a geosynthetic clay liners and geomembrane layer as a hydraulic barrier, 120 cm soil protection layer (Figure 1b). The total waste landfilled was about 9 million tons during its service life, which accounted for more than 60% of the MSW in Hangzhou. The final cover system is fully covered by vegetation and grass on the surface. Real-time meteorological factors including temperature and pressure were obtained through AQM 65 (Aeroqual, New Zealand), which is a compact air quality station designed for precise measurement of ambient pollution and environmental conditions.

2.2 Sampling of gas from landfill cover soil

Soil gas sampling test was conducted on 22nd May and 25th June 2022, at the depth of 0, 30, 60 and 90 cm from the top surface of the cover, by installing stainless steel tubular sampler (diameter=1cm) with perforation at the bottom and a valve at the top. The c/c horizontal distance between each steel tubular sample is 20 cm (Figure 1a). The steel sampling tubes were hammered gently into the cover soil at each depth and they were left at their respective locations for long-term monitoring. Active gas sampling (volume = 1 L) was done with an air pump (GP-2000) and stored in the Tedlar bags (Huibin Instrument Company). The valve was closed off when the sampling was finished. Four multi-integration sensors (YGC-TM, Wuhan Chenyun Technology Co., LTD, China), were installed at the four different soil depths adjacent to the sampling tubes, simultaneously, to measure volumetric soil moisture content and temperature,. The data of the

sensors were read out through a portable monitor meter (TGY-TRY, Wuhan Chenyun Technology Co., LTD). Gas sampling, soil moisture and temperature data were taken at 8:00, 11:00 and 13:00 hrs. In addition, variations of the atmospheric conditions (air humidity, air temperature, and wind speed) during these dates were measured and presented in Table 1 and Figure S1 (supplementary material).

2.3 LFG emission flux measurement

LFG emission flux was measured by a static chamber (height=600mm and diameter=500mm) consisting of a glass cylinder and a steel pedestal and was installed close to the gas sampling tubes as depicted in Figure 1(a). The steel pedestal was hammered into the soil and sealed properly to prevent air from entering. The glass cylinder was put into the groove of the steel pedestal and the installation of the static chamber was finally completed. All the valves were then shut off to allow gas to accumulate in the chamber. Gas was sampled every 60 minutes for a duration of 4 hours. Concentration and composition of the gas samples were determined by gas chromatography (Agilent 7890N, Agilent, USA)-mass spectrometry (GC-MS) and a thermal desorber (Tekmar, Aerotrap 6000, USA) following the processes described by Wang et al. (2019), which is illustrated here briefly for sake of brevity.

Firstly, the gas samples collected from the static chamber were pre-concentrated by cryogenic liquid nitrogen to 1 ml in ventilation, following EPA TO14 (US-EPA, 1999). The cryo trap capillary was a 22 cm part of a 0.53mm id, AT-Q, Q-PLOT column (Alltech Associates), which was used to enhance the trapping of VOCs and consequently provided better chromatographic resolution. A 20 seconds heating pulse was adopted for flash desorption of trapped analytes in the GC column and prevention of extensive deterioration of the cryo trap column. Helium gas (purity= 99.999%) was used as a carrier at flow rate of 1.0 ml/min. The odor samples were desorbed for 5 min at 250 °C using helium gas at the flow rate of 35 mL/min and the trap was desorbed for 5 min. The split ratio

was 1:50. The temperature of inlet, ion source and quadrupole was 250 °C, 230 °C and 150 °C. The temperature program for odors was: initial oven temperature 30 °C, hold for 2 min, and then increase the temperature from 30 °C to 125 °C at 10 °C/min, hold for 30 min. The GC column HP-5 (30m×0.32mm×0.25μm) was set for 3 different temperature ranges, from 28 °C to 60 °C at an increasing rate of 5 °C /min; from 60 °C to 200 °C at an increasing rate of 5 °C/ min; and at 200 °C for 5 min. Electron ionisation (EI) was selected as the ionisation mode at 70eV with the source temperature of 180 °C and the collection electric current of 200 μA. The source and analyzer vacuum pressure were 1×10^{-4} Pa and 1×10^{-6} Pa, respectively. An internal standard method was used to quantify the concentration of VOCs. The chromatographic peaks were identified with the help of the NIST98 library and enhanced by the G170BA substance database. The calibration curve was prepared to obtain the concentration of each VOCs and its peak area, with $R^2 > 0.998$.

Once the concentration was obtained, gas emission rate from LFC was determined by using Eqs. 1 and 2 (Senevirathna et al., 2006).

$$VC_{t+\Delta t} = VC_t + j'S\Delta \quad (1)$$

$$j' = \frac{V}{S}\frac{dC}{dt} \quad (2)$$

where V is the volume of the chamber (m^3). C is the gas concentration (mg/m^3). C_t and $C_{t+\triangle t}$ are the gas concentration (mg/m^3) at time t and $t+\triangle t$ (s), respectively. S is the base area of the chamber (m^2). j' is the gas flux ($mg/m^2/s$). Further, the emission flux (j) has been corrected at atmospheric temperature T (°C) by Eq. 3.

$$j = j' \times \frac{273}{273+T} \quad (3)$$

2.4 Development of coupled numerical model

VOCs migrate from soil to atmosphere takes place via diffusion and advection, which are

controlled by the concentration gradient and total gas pressure, respectively. The transport parameters of VOC in soil including the diffusion coefficient and advection velocity are affected greatly by temperature, pressure gradient, and soil moisture content. Pan et al. (2023) have indicated that air temperature, air humidity, air pressure, wind direction and speed were the major factors that influenced the health risks of VOCs and SVOCs emitted from landfill. This study focuses on the transport processes of VOC inside soil. Air humidity and wind have a more obvious effect on the diffusion of VOCs in air rather than that in soil (Goss and Madliger, 2007; Shen et al., 2018; Pan et al., 2023). Therefore, the attention of this study was paid to the effect of barometric pressure and temperature changes on the transport and emission of VOCs. The one-dimensional numerical modelling developed in this study is based on the following assumptions: (1) Effect of air humidity and wind speed on VOC transport in soil were not considered; (2) Transport of heat and soil moisture, pressure variation were considered in the numerical model; (3) VOCs diffusion and advection follow Fick's second law and Darcy's law, respectively. Atmospheric temperature and pressure variation were monitored and used as the heat and mass transport module boundary conditions. The conceptual model for VOCs transport and emission in a final landfill cover system is shown in Figure 1(b). One-dimensional coupled thermo-hydro-chemical model can be used to describe the transport of VOCs in the soil and the emission into atmosphere (Yan et al., 2020).

2.4.1 Mass transfer equations

The diffusive and advective LFG transport in the cover layer can be described as Eq. 4 (Xie et al., 2018; Wang et al., 2022).

$$D_e \frac{\partial^2 C_a}{\partial z^2} - v \frac{\partial C_a}{\partial z} - \lambda C_a = R_d \frac{\partial C_a}{\partial t} \quad (4)$$

where D_e is the effective VOCs diffusion coefficient, v is advection velocity, λ is the degradation rate of VOCs in the soil, C_a is VOCs concentration, R_d is the retardation factor and z is soil depth.

Governing equation for LFG diffusion in the ground surface air boundary layer can be described by Eq. 5 (Ma et al., 2022).

$$\frac{\partial}{\partial z}\left(D_{eddy}\frac{\partial C_g}{\partial z}\right)=\frac{\partial C_g}{\partial t} \quad (5)$$

where C_g is LFG concentration in air; D_{eddy} is the eddy diffusion coefficient, which increased linearly with depth and can be determined by Eq. 6 (Foken, 2008).

$$D_{eddy}=ku^{*}z+D_g \quad (6)$$

where k is the von Karman constant, and u^{*} is the friction or shear velocity. D_g is the diffusion coefficient in air. The advection process was considered both inside the soil and along the LFC surface. The advection of VOC on the LFC surface was induced by wind velocity (Foken, 2008) whereas inside the soil, it is induced by the gas pressure gradient at the surface and the bottom of the cover (Xie et al., 2018).

It has been demonstrated that LFG concentration in landfill cover fluctuates with time (Barlaz et al., 2004; Wang et al., 2022). No single type of boundary condition is representative of conditions in a wide variety of modern landfills. Therefore, in this study, the bottom boundary conditions for mass transfer are assumed to be constant according to field test results for conservative predictions of VOC transport. Boundary conditions for LFG transport in soil and atmosphere can be described as:

$$C_g(z=z_{BL})=0 \quad (7)$$

$$C_g(z=0^{-})=C_a(z=0^{+}) \quad (8)$$

$$\left.\frac{\partial C_g}{\partial z}\right|_{z=0^{-}}=\left.\frac{\partial C_a}{\partial z}\right|_{z=0^{+}} \quad (9)$$

$$C_a(z=-L)=C_0 \quad (10)$$

where z_{BL} is the atmospheric boundary layer height under neutral or stable atmospheric conditions. L is the depth of the surface vegetation layer. C_0 is the constant VOC concentration at the bottom

boundary.

The adsorption of VOCs by gas phase, water, gas-water interface, and soil solid phase were considered in this paper. The determination of the retardation factor (R_d) is shown in Eq. s4 (supplementary material). Both the effective diffusion coefficient and adsorption retardation factor are related to temperature and soil moisture content change and can be found by Eq. s1 and s4 in S2 (supplementary material).

2.4.2 Governing equations for advection process

Advection of LFG through the final cover soil was assumed to be induced by the accumulation of LFG at the bottom of the cover (Bouazza and Vangpaisal, 2003) and the atmospheric pressure variation (Kim and Benson, 2004; Gebert and Groengroeft, 2006). Pressure gradient between top and bottom of cover layer can be obtained by the following Eq. 11 (Kim and Benson, 2004).

$$\frac{\nabla(k_a P_0 \nabla P_i)}{\mu} = \frac{\theta_a \partial P_i}{\partial t} \tag{11}$$

where P_i is the gas pressure in the soil. P_0 is the average atmospheric pressure (=100 kPa).

The top surface of the cover is connected with the atmosphere and gas pressure at the surface equals barometric pressure. The variation of ground surface barometric pressure (P_a) with time during the day was monitored and data were used as top boundary condition (Eq. 12) for the numerical simulation.

$$P_i(z,t)|_{z=0} = P_a \tag{12}$$

The gas pressure generated by LFG was assumed to be constant because the landfill was closed for fifteen years and the degradation organic matter ceased or was negligible. As Zhan et al. (2017) reported, it is a reasonably appropriate assumption that the generation of LFG reached its steady state after more than ten years of waste degradation. Therefore, the bottom boundary

(z=-0.9m) for pressure was assumed to be a constant pressure boundary (P_L) as Eq. 13.

$$P_i(z,t)|_{z=-L} = P_L \tag{13}$$

Emission flux at the surface of the cover system is comprised of diffusive and advective flux, which can be expressed as Eq. 14.

$$f = -D_a \frac{\partial C_a}{\partial z}\Big|_{z=0} + vC_a(z=0) \tag{14}$$

2.4.3 Governing equations for heat transfer in LFC

Heat conduction in the soil matrix can be determined by Eq. 15 (Ma et al., 2022).

$$\frac{\partial T}{\partial t} = \alpha^* \frac{\partial}{\partial z}\left(\frac{\partial T}{\partial z}\right) \tag{15}$$

where α^* is soil thermal diffusivity, which is highly depended on the soil moisture and can be estimated by the empirical relationship as Eq. (16) (Arkhangelskaya and Lukyashchenko, 2018).

$$\alpha^* = \alpha_0 + a * \exp\left[-0.5\left(\frac{\ln(\frac{\theta_w}{\theta_{w0}})}{b}\right)^2\right] \tag{16}$$

where α_0 is the thermal diffusivity of dry soil, θ_{w0} is the water content when the thermal diffusivity of soil is maximum, a is the difference between the highest thermal diffusivity at the optional water content $\theta_{w0,}$ and the thermal diffusivity of dry soil and b is the half-width of the peak of the $\kappa(\theta)$ curve.

It is indicated by Wang et al. (2017) that the spatial patterns and temporal evolutions of the ground surface temperature are similar to those of surface air temperature, with the maximum difference in summer (3.9°C) and the minimum difference in winter (0.6°C). Therefore, the monitored time variation of ground surface air temperature (T_a) during one year was used as top boundary condition (Eq. 17) for heat migration study.

$$T(z,t)|_{z=0} = T_a \tag{17}$$

The temperature at the bottom (z=-L_s) of the cover is assumed to be a constant temperature (T_0) (Eq. 18) as its variation is negligible (Ma et al., 2022).

$$T(z,t)|_{z=-L} = T_0 \tag{18}$$

2.4.4 Governing equations for soil moisture transport

One-dimensional soil moisture transport can be described by Richard's equation as in Eq. 19 (Yan et al., 2020, 2022).

$$C(H_p)\frac{H_p}{\partial t} = \frac{\partial}{\partial z}[K(H_p)\frac{\partial H_p}{\partial z}] - \frac{\partial K(H_p)}{\partial z} + \Phi \tag{19}$$

where H_p is the pressure head, $K(H_p)$ is the hydraulic conductivity, $C(H_p)$ is the water capacity or the slope of the soil water retention curve, which is expressed in Eq. 20.

$$C(H_p) = \frac{\partial \theta_w}{\partial H_p} \tag{20}$$

The surface soil moisture content (soil water tension) was related to the air humidity, which can be described as (Or and Wraight, 2000; Goss et al., 2007):

$$h = RTM_W^{-1}\rho_W \ln(RH) \tag{21}$$

where h is the pressure head at the soil surface. R is the gas constant. T is the absolute temperature. M_w is the molecular weight of water and ρ_w is the density of liquid water. RH is the air humidity, which was also measured and shown in Figure S1(a) in the supplementary materials. Generally, air humidity will impact the VOC emission process by affecting the moisture content at the soil surface. However, Goss and Madliger (2007) indicated that when air humidity increased from 39% to 76% (range of air humidity found in present study), soil moisture content only increased by 0.03 (m^3 water/ m^3 soil). Therefore, the effect of air humidity on the emission of VOCs will not be investigated in detail in the present paper, which will be further studied in the future.

The Brooks and Corey retention models were used to obtain unsaturated hydraulic

conductivity, presented in S3 in the supplementary material.

The coupled mathematical model was solved numerically by the finite element method by using COMSOL Multiphysics® (version 5.6) (COMSOL, 2014). Loam clay was chosen for the numerical simulation in accordance with site situation. The Richard's Equation interface was used for moisture transport modeling and unsaturated parameters used in this analysis (Eqs. s10-s13) were presented in Table s1 in the supplementary material. The coefficient form PDE interface was used for the simulation of pressure, mass and heat transfer. The parameters of benzene and dichloromethane were shown in Table 2. It is indicated that the spatial patterns and temporal evolutions of ground surface temperature are similar to those of surface air temperature (Wang et al., 2017). The functions were then used based on monitoring data as the boundary conditions for pressure and temperature variation, corresponding to P_a and T_a in Eq. (12) and Eq. (17), respectively. The inbuilt extremely fine physics-controlled mesh was considered where the maximum element size of the meshes is 0.009m and includes 100 edge elements and 2 vertex elements. Richard's equation, thermal transfer, pressure change, and mass transfer were solved step by step by using the inbuilt solver.

3 Results and discussions

3.1 Composition and concentration of VOCs with field test

Depth-wise variation in composition and concentration of investigated VOCs in the final cover of the landfill are depicted in Figure S2 (a) and (b) in May and June, respectively, at different times of the day. Also, total VOC concentration profiles in May and June are shown in Figure S3(a) and (b), respectively. VOC concentrations in soil were dominated by aromatic compounds (benzene, o-xylene, styrene, P-m-xylene, ethylbenzene, and methylbenzene) and halogenated hydrocarbons (tetrachloroethylene, dichloromethane, dichloroethylene, trichloromethane and dibromoethane). The VOC concentration varied with time and soil depth, as observed from these

figures. It is noticed from Figure S2 that the concentration in the soil was relatively high although the landfill has been closed for more than fifteen years. The maximum total VOC concentration was reached at the depth of 90 cm in May. In May, the total VOCs concentration at the surface and at the depth of 30, 60 and 90 cm of the cover ranges 100-632 $\mu g/m^3$, 150-350 $\mu g/m^3$, 110-790 $\mu g/m^3$, and 650-1350 $\mu g/m^3$, respectively (refer to Figure S2a). On the other hand, it can be noticed from Figure S2(b) the total VOC concentration at the surface and at the depth of 30, 60 and 90 cm were 648-943 $\mu g/m^3$, 630-810 $\mu g/m^3$, 650-890 $\mu g/m^3$, and 400-850 $\mu g/m^3$, respectively, in June. Compared with the results in May, total VOCs concentration in June at four depths showed less variation. It is mainly because the high temperature in June increased the gas diffusion coefficients of VOCs in soil. Therefore, variation of concentration profiles decreased in June.

It is indicated from Figure S2 that the concentration of benzene at the surface of the cover ranges from 11.4 to 144 $\mu g/m^3$ in May. The maximum concentration of benzene emitting from the landfill cover surface is four times greater than the reference concentration (RfC) for benzene, which is 30 $\mu g/m^3$ based on hematological effects in humans. The RfC is an estimation (with uncertainty spanning perhaps an order of magnitude) of continuous inhalation exposure to the human population (including sensitive groups) that is likely to be without appreciable risk deleterious noncancer effects over a lifetime (US EPA, 2009). The maximum concentration of benzene was detected at a depth of 90 cm, reaching 255 $\mu g/m^3$ at 13:00 hrs, which was more than 8 times greater than the RfC. It should also be noted that dichloromethane (DCM) dominated VOCs concentration both in May and June. The ranges of DCM concentration at depth of 90 cm were 95-440 $\mu g/m^3$ in May and 156-327 $\mu g/m^3$ in June, which were 2-6.8 times greater than toluene. Yao et al. (2019) also found that the concentration of DCM is the highest among the detected halogenated compounds, reaching 15123 $\mu g/m^3$ in the defects of the temporal cover at the

same landfill investigated in this study. Comparison between the results obtained at the final cover through this study and the temporary cover by Yao et al. (2019) indicated that the degradation of the MSW is a long-term process and landfill will be a long-term source of VOC emission (Zhan et al., 2017). The concentration of DCM at the surface of the final cover system monitored in this study is 1.3-114 μg/m³, which is similar with the results reported by Duan et al. (2021), where the authors reported that DCM concentration spans from 0.3 to 150 μg/m³ at the surface of temporal or final cover. DCM can be absorbed through the skin and its long-term exposure via inhalation will result in liver toxicity, liver cancer, and lung cancer (US EPA, 2011).

It can be observed from Figure 2 that the total VOC flux emitted from the cover surface was 0.0124 and 0.0625 μg/m^2/s in May and June, respectively. DCM dominated VOCs emission flux both in May and June, followed by P-m-xylene and tetrachloroethylene in May and June, respectively. The emission flux of the DCM comprised 51.8% and 28% of the total VOCs emission flux in May and June, respectively. The emission rate of the DCM in May is 0.00968 μg/m^2/s (≈ 8.4×10^{-4} g/m^2/d), which is 1-4 orders of magnitude higher than that obtained by Schuetz et al. (2003) at a French landfill. The DCM was also one of the most common species detected from landfill by Liu et al. (2017), and with a composition of 32% among halocarbon emissions. Based on the monitoring study by Liu et al. (2017) at the three anaerobic MSW landfills in China, it is reported that the DCM concentration at working face ranges from 9.4 to 342.8 μg/m^2/s, which is 3-6 orders of magnitude higher than the results obtained in the present study. It is reasonable because DCM was mainly volatilized directly from MSW components, such as plastics and adhesives (Yao et al., 2019; Duan et al., 2021). Besides, the results found in this study were monitored on the final cover consisting of soil layers and geosynthetics, which are diffusion barriers and sorptive carriers for DCM transport (Schuetz et al., 2003; Wang et al., 2022). The

higher emission flux of DCM than other types of VOCs were mainly attributed to two reasons. Firstly, the concentration of DCM at the bottom of the cover system was the greatest among all the VOCs tested. Secondly, the properties of DCM, including the Henry's constant, diffusion coefficient in air are diffident from other types of VOCs. The difference between the emission flux of benzene and DCM will be discussed in detail through numerical modelling.

3.2 Validation of the results obtained from numerical modelling

Results obtained from the numerical modelling were validated with the field tests results of the soil moisture content (soil water-filled porosity), soil temperature and VOC concentration. Field test results obtained at 8:00 and 13:00 hrs were chosen for the verification. The results for the verification of soil moisture content, temperature profiles, benzene and DCM concentration profiles were presented in Figures 3(a)-(d), respectively. It can be noticed that the proposed numerical modelling results are in good agreement with those obtained from the field monitoring. However, it should also be noted that concentration of benzene at the depth of z=-0.3m, at 8:00 am obtained by numerical modelling deviated from field monitoring results. This can be attributed to dilution of by air during transportation and storage in teldar bags before testing by GC-MS, leading to lower concentration than that obtained from numerical modelling.

Figure 3(d) also indicated that at 08:00 am, the DCM concentration from z=-0.6 to z=-0.2 approaches zero, which is less than the concentration at z=-0.9 and z=0. The concentration gradient along soil depth controls the diffusion process of VOCs. When VOC concentration at the soil surface is more significant than that at the shallow depth of soil, VOC will diffuse from the surface into the shallow depth of soil. Therefore, VOCs concentration in soil varies with time, which can also be found in Figure S3. Similar result was also reported by Schuetz et al. (2003) in a final landfill cover in France. It was shown that a decrease occurred for non-methane organic compounds concentrations between 60- and 80-cm soil depths.

3.3 VOCs emission flux from the final cover predicted by the numerical model

3.3.1 Effect of daily ground surface air temperature variation

Figure 4 depicts the variation of temperature and calculated surface diffusive emission flux of benzene and DCM during a day in four seasons by numerical modelling. The monitored concentration ranges for benzene and DCM at a depth of z=-0.9m are 3.1-255.3 μg/m^3 and 95-327 μg/m^3, respectively. The tested concentration ranges for benzene and DCM at the surface of the cover are 0-144 μg/m^3 and 2-171 μg/m^3, respectively. Therefore, the concentration boundaries of benzene and DCM at the depth of z=-0.9m and z=0m for numerical modelling were chosen to be 150 μg/m^2/day and 30 μg/m^2/day, respectively. Loam clay was chosen for the numerical simulation. It is demonstrated that temperature variation during a day can have great influence on the emission flux of benzene and DCM. VOCs emission flux increases with the increase of temperature. The emission flux during a day changes consistently with the changes of temperature. Temperature difference during the day in spring is the maximum (ΔT＞20 ℃) among the four seasons. The diffusive emission flux of benzene and DCM reaches its maximum at the highest temperature, which occurs at 15:00 hrs in four seasons (Figure 4). The average VOC emission flux was the highest in summer, followed by that in spring, autumn, and winter. The variation of emission flux is similar to the temperature trends. Emission flux of benzene in spring ranges from 2000 to 2220 μg/m^2/day. The difference in emission flux in spring induced by temperature variation is 220 μg/m^2/day, which is the highest in the four seasons. This is because the maximum temperature difference in spring, which also results in the maximum VOCs emission flux reached in spring (Figure 4). Although the highest temperature was in summer, the maximum emission flux was reached in spring (≈2220 μg/m^2/day for benzene). The maximum temperature difference induced the maximum emission in spring during the same time. The emission flux of benzene in

summer ranges from 2080 to 2200 μg/m^2/day. The maximum difference of the benzene emission flux in summer is 120 μg/m^2/day, which is 1.8 times less than that in spring. Benzene emission flux in winter varied between 1920 and 2060 μg/m^2/day, which was the lowest owing to the lowest temperature in winter. The obtained emission flux in this study is found to be within the range of VOCs emission flux (875-3750 μg/m^2/day) reported by Guo et al. (2015) at a living area contaminated by VOCs, indicating the reliability of the numerical results obtained in this study.

The patterns of the daily DCM emission are identical to that of benzene, following a similar trend with daily temperature change (Figure 4). It can be indicated from Figure 4 that the emission of DCM is higher than that of benzene. The emission flux of DCM in spring varied between 2120 to 2360 μg/m^2/day. The maximum emission of DCM (=140 μg/m^2/d) is higher than that of benzene. The lowest emission flux of DCM was also in winter, ranging from 2060 to 2200 μg/m^2/d. The higher emission of DCM compared with benzene in this study was mainly due to higher diffusion coefficient of DCM. The diffusion coefficient of DCM is approximately 1.2 times greater than of benzene. The Henry's constant of DCM is 2.15 times less than that of benzene, which indicates that the dissolved amount of DCM is smaller than that of benzene under the same equilibrium partial pressure. Besides, based on field tests at a French landfill, Scheutz et al. (2008) indicated that halogenated hydrocarbons, including DCM were not degradable in the cover soil, while aromatics, including benzene, were degradable at a relatively higher rate.

Consequently, the emission of DCM is more than that of benzene. The daily amplitudes of benzene and DCM were similar. In spring, the fluctuations of benzene and DCM were 220 μg/m^2/d and 240 μg/m^2/d, respectively. In winter, the fluctuation amplitudes for both benzene and DCM were 140 μg/m^2/d, which indicates that the amplitude of daily temperature mainly determined the magnitude of fluctuation. The temperature-dependent diffusion in soil mainly caused the variation

406 of diffusive VOC emissions. The diffusivity of VOCs in soil was dependent on soil temperature
407 (Eqs. s1-s3). Thus, the variation of the VOCs concentration follows the same trend of temperature
408 change, which was controlled mainly by the thermal diffusivity coefficient of soils.

409 *3.3.2 Effect of daily barometric pressure changes on VOCs emission*

410 Figure 5 shows the estimated surface advective flux of benzene during a day in four seasons.
411 It can be concluded from Figure 5 that the fluctuation of barometric pressure has a great influence
412 on the advective emission of benzene. Advective emission of benzene increases with the decrease
413 of atmospheric pressure, showing a reverse trend with barometric pressure variation. In addition,
414 the fluctuation of benzene advective emission lags behind atmospheric pressure changes. The
415 highest atmospheric pressure during a day in spring occurred at 15:00 hrs, while the lowest benzene
416 emission flux occurred at 16:00 hrs. With the increase of barometric pressure during 18:00 to 20:00
417 hrs in spring, the emission flux of benzene decreased immediately (Figure 7a). When the
418 barometric pressure decreases, the pressure difference increases because the pressure at the bottom
419 boundary is assumed to be constant (Eq. 13), leading to increasing advective emission flux. It is
420 demonstrated from Figure 5 that the amplitude of barometric pressure fluctuations has a significant
421 impact on the advective emission of benzene. The maximum difference of barometric pressure in
422 spring is 8 hPa, followed by 4 hPa in winter, 3.3 hPa in autumn, and 3 hPa in summer. The
423 correspondingly advective emission flux difference during a day of benzene in spring is the
424 highest, followed by that in winter, autumn, and summer, with similar results. In response to the
425 fluctuation of barometric pressure, a vertical pressure gradient was developed within the cover
426 soil. Thus, the variation of advective velocity was resulted by the fluctuated vertical pressure
427 gradient. It is demonstrated that the variation of the advective emission flux of benzene induced
428 by atmospheric pressure can reach three orders of magnitude (Figure 5). The advective emission

flux in spring decreased from -5000 μg/m^2/day to 0 μg/m^2/day, and then increased gradually to 5000 μg/m^2/day (negative sign indicates inward flux from atmosphere into the cover soil) in the reverse direction. Previous studies have also shown that the emission flux of LFG can vary by several orders of magnitude at the same landfill (Schroth et al., 2012). It is suggested by Xu et al. (2014) that such large variations in LFG emissions reported in those earlier studies were due to barometric pressure fluctuations. The results found by the proposed numerical solution in this study also confirms the findings of Xu et al. (2014).

Moreover, advective transport of benzene from the atmosphere into cover soil will result in the accumulation of benzene in the shallow cover soil. Therefore, benzene concentration at the shallow depth can be greater than that in a deeper depth (z=-0.9m). Furthermore, back-diffusion of LFG from the atmosphere or shallow depth to deep depth of cover soil will occur. The numerical simulation results explain the results found by the field test shown in Figure S2(a) that the total VOC concentration at the depth z=0 is about 3 times greater than that at the depth of z=-0.3m at 8:00 hr. Similarly, in Figure S2(b), the concentration of total VOC at the depth of z=-0.3m is 1.8 times greater than that at a depth of z=-0.9m. VOCs would diffuse from the shallow depth of soil into the deeper depth by back-diffusion under this circumstance. The results highlight that diffusion and advective flow contribute significantly to the VOCs transport process. It also implies that emission flux estimated from the static chamber method may be erroneous due to not allowing the emission of LFG induced by pressure fluctuation as it was covered with an airtight cover. Also, there may be some loss of gas due to preferential flow at the gas chamber and soil interface.

3.3.3 Estimation of annual emission flux of VOCs

Figures 6(a) and (b) show the variation of temperature and pressure during the entire year by field test, and the estimated daily VOC emission flux during one year by numerical modeling,

respectively. It can be observed from Figure 6(b) that the absolute value of VOCs emission flux ranges from 0-2100 ug/m^2/s, which falls within the range of global non-methane VOCs emission flux obtained by Manheim et al. (2021). The response of VOCs emission flux to the fluctuation in atmospheric temperature and pressure is much clearer on month scales (Figure 6a). The daily emission of diffusive flux during a year shows similar trends with the variation of temperature, while the daily advective flux shows inverse trends with the variation of barometric pressure. Furthermore, the emission flux of diffusive flux fluctuates simultaneously with the changes of temperature, while the emission of advective flux lags behind the fluctuation of barometric pressure. The daily diffusive emission flux of benzene and DCM reaches its maximum in June (the 210^{th} day), when the maximum temperature also occurred in June. Daily diffusive fluxes of VOC increased with the increase of daily average temperature because the increases of atmospheric temperature induced the rise of the soil temperature and consequently increased the gas diffusion coefficient (D_e) in soils. The highest advective flux occurred in May while the lowest atmospheric pressure occurred in June. The average daily diffusive emission flux of benzene varied between 1700-1990 μg/m^2/d, which is 30-40 μg/m^2/d less than that of DCM, ascribing to the difference in D_e. The high diffusive emission of VOCs was mainly in spring and summer, while the low diffusive emission was mainly in autumn and winter. High emission of advective emission was mainly in spring and summer, while low advective emission was mainly in autumn and winter. Advective emission flux were strongly inhibited when barometric pressure increased in autumn and winter due to the decrease of pressure difference. Shen et al. (2018) also observed a strong negative correlation between landfill gas emission and barometric pressure changes based on field monitoring. Emission fluxes were strongly enhanced when barometric pressure decreased in spring and summer, corresponding to increased pressure gradient along soil depth. The daily average

advective emission flux of benzene and DCM is similar, ranging from -2000-750 μg/m^2/day. The amplitude of variation for average daily VOCs emission is smaller than the one-day emission shown in Figures 6 and 7. This is because the dramatic temperature fluctuation during a day exceeds the average daily variation amplitude during one year. It should also be noted that for advective emission of VOCs, the direction of advective flux is mainly from the atmosphere into the cover soil during winter shown in Figure 6(b). While in spring and summer, the advective emission of VOCs was mainly from the landfill cover soil into the atmosphere. This is because the atmospheric pressure in winter is the highest during the year (Figure 6(a)). And the atmospheric pressure is more significant than that in the cover soil, which would result in the advective transport of VOCs from the atmosphere into the soil.

4 Conclusion

The concentration profiles of VOC at different depths of cover soil were obtained through field test. The numerical simulation was conducted to investigate the influence of temperature and barometric pressure fluctuation on the diffusive emission and advective emission of VOCs. Main conclusions are:

(1) Field monitoring shows that VOCs concentrations in soil were dominated by aromatic compounds and halogenated hydrocarbons. DCM dominated VOCs concentration and emission flux both in May and June. Furthermore, the emission flux of the DCM comprised 51.8% and 28% of the total VOCs emission flux in May and June, respectively.

(2) Numerical simulation shows that daily temperature and barometric pressure variation have crucial effect on diffusive and advective VOCs emissions, respectively. VOCs emission flux increases with the increase in temperature and follows similar trends with the variation of temperature synchronously. Higher temperature fluctuation will result in higher diffusive emissions of VOCs. The variation of advective emission also shows an inverse fluctuation and

lags that of the barometric pressure variation. The advective VOCs transport from the atmosphere into soil occurs when the pressure inside the cover soil is greater than that in the atmosphere. It will result in the accumulation of VOC in the shallow depth of soil and thus back-diffusion occurs.

(3) The daily diffusive emission flux of VOCs reaches its maximum in June and the lowest advective flux occurred in May due to the fluctuation of temperature and barometric pressure during the year. High diffusive emission of VOCs was mainly in spring and summer. The direction of advective flux is from the atmosphere into the cover soil during winter.

(4) It is indicated that the emission of VOC from final covers induced by atmospheric factors, including temperature and pressure is non-negligible and should be considered when assessing the risks of landfill and estimating LFG emission budget reasonably. Fluctuation of pressure and temperature plays a more significant role on LFG emission than they were thought in previous studies. The results found in this study can give new insight into designing climate-adaptive landfill covers.

Data Availability Statements

Some or all data, models, or code that support the findings of this study are available from the corresponding author upon reasonable request.

Acknowledgements

The financial supports provided by the “Pioneer” and “Leading Goose” R&D Program of Zhejiang (Grant No. 2022C03051), National Natural Science Foundation of China (Grant Nos. 52278375，41977223 and 41931289), and Natural Science Foundation of Zhejiang province (Grant No. LR20E080002) are greatly acknowledged.

Notation List

a difference between the highest thermal diffusivity at the optional water content and the thermal diffusivity of dry soil.

b half-width of the peak of the $\kappa(\theta)$ curve.

C gas concentration in the static chamber.

C_a VOCs concentration in soil.

C_g VOCs concentration in air.

C_0 constant VOCs concentration at the bottom boundary.

$C(H_p)$ water capacity or the slope of the soil water retention curve.

d_g soil structure characterizing parameter.

D_{eddy} eddy diffusion coefficient.

D_e (T) effective diffusion coefficient of VOCs in soil at temperature T.

D_g (T) diffusion coefficients of VOCs in air at temperature T.

D_w (T) diffusion coefficients of VOCs in water at temperature T.

D_{g0} diffusion coefficient of VOCs in air at temperature T_0.

D_{w0} diffusion coefficient of VOCs in water at temperature T_0.

f_{oc} soil's organic carbon fraction.

H_p pressure head.

$j^{'}$ gas flux.

j corrected gas flux at environment temperature T.

k von Karman constant.

K_H Henry's gas constant.

544 K_{H0} Henry's constant at T_0.

545 $K(H_p)$ hydraulic conductivity.

546 K_s saturated hydraulic conductivity.

547 k_a permeability of VOCs through soil.

548 K_d distribution coefficient.

549 K_{oc} soil organic carbon-water partition coefficient.

550 k_{oc0} sorption coefficient at T_0.

551 L depth of the surface vegetation layer.

552 P_i gas pressure in the soil.

553 P_0 average atmospheric pressure.

554 R_d retardation factor.

555 S base area of the chamber.

556 Se effective saturation.

557 u^* friction or shear velocity.

558 V volume of the chamber.

559 v advection velocity.

560 z soil depth.

561 z_{BL} atmospheric boundary layer height.

562 λ degradation rate of VOCs in soil.

563 θ_a air-filled porosity of soil.

564 θ_w water-filled porosity of soil.

565 ε total porosity of soil.

566 $\triangle H_{sorp}$ enthalpy of sorption.

567 R ideal gas constant.

568 $\triangle H_{aw}$ enthalpy of air-water partitioning.

569 μ dynamic viscosity coefficient of VOCs.

570 α^* soil thermal diffusivity.

571 ρ_b dry density of soil.

572 α_0 thermal diffusivity of dry soil.

573 θ_{w0} water content at when the thermal diffusivity of soil is maximum.

574 α, l, n empirical constants.

575 θ_r and θ_s residual and saturated volumetric water content of soil, respectively.

576

References

Arkhangelskaya, T., & Lukyashchenko, K. (2018). Estimating soil thermal diffusivity at different water contents from easily available data on soil texture, bulk density, and organic carbon content. Biosystems Engineering, 168, 83-95. https://doi.org/10.1016/j.biosystemseng.2017.06.011

Barlaz, M. A., Green, R. B., Chanton, J. P., Goldsmith, C. D., & Hater, G. R. (2004). Evaluation of a biologically active cover for mitigation of landfill gas emissions. Environmental Science & Technology, 38(18), 4891-4899. https://doi.org/10.1021/es049605b

Brooks, R. H., & Corey, A. T. (1966). Properties of porous media affecting fluid flow. Journal of the irrigation and drainage division, American Society of Civil Engineers, 92(IR2), 61-88.

Bouazza, A. & Vangpaisal, T. (2003). An apparatus to measure gas permeability of geosynthetic clay liners. Geotextiles and Geomembranes, 21, 85-101. https://doi.org/10.1016/S0266-1144(02)00058-4

Chiou, C. T., & Shoup, T. D. (1985). Soil sorption of organic vapors and effects of humidity on sorptive mechanism and capacity. Environmental Science & Technology, 19(12), 1196-1200. https://doi.org/10.1021/es00142a010

COMSOL. (2014). COMSOL Multiphysics, 5th edn. http://cn.comsol. com/

Delle Site, A. (2001). Factors affecting sorption of organic compounds in natural sorbent/water systems and sorption coefficients for selected pollutants. A review. Journal of Physical and Chemical Reference Data, 30(1), 187-439. https://doi.org/10.1063/1.1347984

Duan, Z., Scheutz, C., & Kjeldsen, P. (2021). Trace gas emissions from municipal solid waste landfills: A review. Waste Management, 119, 39-62. https://doi.org/10.1016/j.wasman.2020.09.015

Feng, S., Ng, C.W.W., Leung, A.K., Liu, H.W. (2017a). Numerical modelling of methane oxidation efficiency and coupled water-gas-heat reactive transfer in a sloping landfill cover. Waste Management, 68, 355-368. https://doi.org/10.1016/j.wasman.2017.04.042

Feng, S., Leung, A. K., Ng, C. W. W., & Liu, H. W. (2017b). Theoretical analysis of coupled effects of microbe and root architecture on methane oxidation in vegetated landfill covers. Science of the Total Environment, 599, 1954-1964. https://doi.org/10.1016/j.scitotenv.2017.04.025

Feng, S., Leung, A. K., Liu, H. W., Ng, C. W. W., Zhan, L. T., & Chen, R. (2019). Effects of thermal boundary condition on methane oxidation in landfill cover soil at different ambient temperatures. Science of the Total Environment, 692, 490-502. https://doi.org/10.1016/j.scitotenv.2019.07.108

Foken, T. (2008). Micrometeorology (Vol. 2). Berlin: Springer. https://link.springer.com/content/pdf/10.1007/978-3-540-74666-9.pdf

Gebert, J., & Groengroeft, A. (2006). Passive landfill gas emission–influence of atmospheric pressure and implications for the operation of methane-oxidising biofilters. Waste Management, 26(3), 245-251. https://doi.org/10.1016/j.wasman.2005.01.022

Goss, K. U., & Madliger, M. (2007). Estimation of water transport based on in situ measurements of relative humidity and temperature in a dry Tanzanian soil. Water Resources Research, 43(5). https://doi.org/10.1029/2006WR005197

Guo, Y., Holton, C., Luo, H., Dahlen, P., Gorder, K., Dettenmaier, E., & Johnson, P. C. (2015). Identification of alternative vapor intrusion pathways using controlled pressure testing, soil gas monitoring, and screening model calculations. Environmental Science & Technology, 49(22), 13472-13482. https://doi.org/10.1021/acs.est.5b03564

Hamamoto, S., Moldrup, P., Kawamoto, K., Wickramarachchi, P. N., Nagamori, M., & Komatsu, T. (2011). Extreme compaction effects on gas transport parameters and estimated climate gas exchange for a landfill final cover soil. Journal of Geotechnical and Geoenvironmental Engineering, 137(7), 653-662. https://doi.org/10.1061/(ASCE)GT.1943-5606.0000459

Huang, B., Lei, C., Wei, C., & Zeng, G. (2014). Chlorinated volatile organic compounds (Cl-VOCs) in environment-sources, potential human health impacts, and current remediation technologies. Environment International, 71, 118-138. https://doi.org/10.1016/j.envint.2014.06.013

Hu, J., Lan, J. W., Chen, Y. M., Xu, W. J., Meng, M., Ma, P. C., & Ke, H. (2023). Foam Flow Model of Municipal Solid Waste and Its Application in Landfill Gas Pressure Prediction. Journal of Geotechnical and Geoenvironmental Engineering, 149(3), 04023004. https://doi.org/10.1061/JGGEFK.GTENG-10602

Kim, H., & Benson, C. H. (2004). Contributions of advective and diffusive oxygen transport through multilayer composite caps over mine waste. Journal of Contaminant Hydrology, 71(1-4), 193-218. https://doi.org/10.1016/j.jconhyd.2003.10.001

Kissas, K., Kjeldsen, P., Ibrom, A., & Scheutz, C. (2023). The effect of barometric pressure changes on the performance of a passive biocover system, Skellingsted landfill, Denmark. Waste Management, 156, 216-226. https://doi.org/10.1016/j.wasman.2022.11.029

Lei, X., Cheng, H., Peng, J., Jiang, H., Lyu, X., Zeng, P., Wang, Z., & Guo, H. (2021). Impact of long-range atmospheric transport on volatile organic compounds and ozone photochemistry at a regional background site in central China. Atmospheric Environment, 246, 118093. https://doi.org/10.1016/j.atmosenv.2020.118093

Liu, Y., Lu, W., Dastyar, W., Liu, Y., Guo, H., Fu, X., Li, H., Meng, R., Zhao, M., & Wang, H. (2017). Fugitive halocarbon emissions from working face of municipal solid waste landfills in China. Waste Management, 70, 149-157. https://doi.org/10.1016/j.wasman.2017.08.042

Ma, E., Liang, X., Zhang, J., & Zhang, Y. K. (2022). Dynamics in Diffusive Emissions of Dissolved Gases from Groundwater Induced by Fluctuated Ground Surface Temperature. Environmental Science & Technology, 56(4), 2355-2365. https://doi.org/10.1021/acs.est.1c06009

Massmann, J. W. (1989). Applying groundwater flow models in vapor extraction system design. Journal of Environmental Engineering, 115(1), 129-149. https://doi.org/10.1061/(ASCE)0733-9372(1989)115:1(129)

Manheim, D. C., Yeşiller, N., & Hanson, J. L. (2021). Gas emissions from municipal solid waste landfills: a comprehensive review and analysis of global data. Journal of the Indian Institute of Science, 101(4), 625-657. https://doi.org/10.1007/s41745-021-00234-4

Mohammad, A., Osinski, P., Koda, E., & Singh, D. N. (2021). A case study on establishing the state of decomposition of municipal solid waste in a bioreactor landfill in India. Waste Management & Research, 39(11), 1375-1388. https://doi.org/10.1177/0734242X211045607

Mohammad, A., Singh, D. N., Podlasek, A., Osinski, P., & Koda, E. (2022). Leachate characteristics: Potential indicators for monitoring various phases of municipal solid waste decomposition in a bioreactor landfill. Journal of Environmental Management, 309, 114683. https://doi.org/10.1016/j.jenvman.2022.114683

Mu, M., Zhang, X., Yu, G., Xu, R., Liu, N., Wang, N., Chen, B., & Dai, C. (2022). Effective absorption of dichloromethane using deep eutectic solvents. Journal of Hazardous Materials, 439, 129666. https://doi.org/10.1016/j.jhazmat.2022.129666

Ng, C. W. W., Chen, Z. K., Coo, J. L., Chen, R., & Zhou, C. (2015a). Gas breakthrough and emission through unsaturated compacted clay in landfill final cover. Waste Management, 44, 155-163. https://doi.org/10.1016/j.wasman.2015.06.042

Ng, C. W., Liu, J., Chen, R., & Xu, J. (2015b). Physical and numerical modeling of an inclined three-layer (silt/gravelly sand/clay) capillary barrier cover system under extreme rainfall. Waste Management, 38, 210-221. https://doi.org/10.1016/j.wasman.2014.12.013

Ng, C. W. W., Zhang, Q., Zhou, C., & Ni, J. (2022). Eco-geotechnics for human sustainability. Science China Technological Sciences, 1-37. https://doi.org/10.1007/s11431-022-2174-9

Pan, Q., Liu, Q. Y., Zheng, J., Li, Y. H., Xiang, S., Sun, X. J., & He, X. S. (2023). Volatile and semi-volatile organic compounds in landfill gas: Composition characteristics and health risks. Environment International, 107886. https://doi.org/10.1016/j.envint.2023.107886

Pré, P., Delage, F., Faur-Brasquet, C., & Le Cloirec, P. (2002). Quantitative structure–activity relationships for the prediction of VOCs adsorption and desorption energies onto activated carbon. Fuel Processing Technology, 77, 345-351. https://doi.org/10.1016/S0378-3820(02)00071-1

Rowe, R. K., Quigley, R. M., Brachman, R.W. and Booker, J.R. (2004). Barrier systems for waste disposal. Spon Press, London.

Schwarzenbach, R.P., Gschwend, P.M., Imboden, D.M., 2003. Environmental Organic Chemistry. 2nd ed. John Wiley & Sons Inc., New Jersey.

Schuetz, C., Bogner, J., Chanton, J., Blake, D., Morcet, M., & Kjeldsen, P. (2003). Comparative oxidation and net emissions of methane and selected non-methane organic compounds in landfill cover soils. Environmental Science & Technology, 37(22), 5150-5158. https://doi.org/10.1021/es034016b

Scheutz, C., Bogner, J., Chanton, J. P., Blake, D., Morcet, M., Aran, C., & Kjeldsen, P. (2008). Atmospheric emissions and attenuation of non-methane organic compounds in cover soils at a French landfill. Waste management, 28(10), 1892-1908. https://doi.org/10.1016/j.wasman.2007.09.010

Schroth, M. H., Eugster, W., Gómez, K. E., Gonzalez-Gil, G., Niklaus, P. A., & Oester, P. (2012). Above-and below-ground methane fluxes and methanotrophic activity in a landfill-cover soil. Waste Management, 32(5), 879-889. https://doi.org/10.1016/j.wasman.2011.11.003

Senevirathna, D. G., Achari, G., & Hettiaratchi, J. P. (2006). A laboratory evaluation of errors associated with the determination of landfill gas emissions. Canadian Journal of Civil Engineering, 33(3), 240-244. https://doi.org/10.1139/l05-111

Shen, S., Chen, Y., Zhan, L., Xie, H., Bouazza, A., He, F., & Zuo, X. (2018). Methane hotspot localization and visualization at a large-scale Xi'an landfill in China: effective tool for landfill gas management. Journal of Environmental Management, 225, 232-241. https://doi.org/10.1016/j.jenvman.2018.08.012

USEPA. (2013) EPA. On-line tools for site assessment calculation. Accessed 25th January, 2013 Waitz, M.F.W., Frei

U.S. Environmental Protection Agency. (2009). Integrated risk information system (IRIS) on benzene. Washington (DC): National Center for Environmental Assessment, Office of Research and Development

U.S. Environmental Protection Agency. (2011). Toxicological Review of DCM (Methylene Chloride) (EPA/635/R-10/003F). Washington (DC): National Service Center for Environmental Publications, Office of Research and Development.

US EPA. (1996). Soil Screening Guidance: User's Guide, Second Edition. Office of Emergency and Remedial Response U.S. Environmental Protection Agency Washington, DC 20460

Wang, Y., Hu, Z. Z., & Yan, F. (2017). Spatiotemporal variations of differences between surface air and ground temperatures in China. Journal of Geophysical Research: Atmospheres, 122(15), 7990-7999. https://doi.org/10.1002/2016JD026110

Wang, Q., Zuo, X., Xia, M., Xie, H., He, F., Shen, S., Bouazza, A., & Zhu, L. (2019). Field investigation of temporal variation of volatile organic compounds at a landfill in Hangzhou, China. Environmental Science and Pollution Research, 26(18), 18162-18180. https://doi.org/10.1007/s11356-019-04917-5

Wang, Q., Gu, X., Tang, S., Mohammad, A., Singh, D. N., Xie, H., Chen, Y., Zuo, X., & Sun, Z. (2022). Gas transport in landfill cover system: A critical appraisal. Journal of Environmental Management, 321, 116020. https://doi.org/10.1016/j.jenvman.2022.116020

Xie, H., Wang, Q., Yan, H., & Chen, Y. (2017). Steady-state analytical model for vapour-phase volatile organic compound (VOC) diffusion in layered landfill composite cover systems. Canadian Geotechnical Journal, 54(11), 1567-1579. https://doi.org/10.1139/cgj-2016-0293

Xie, H., Wang, Q., Bouazza, A., & Feng, S. (2018). Analytical model for vapour-phase VOCs transport in four-layered landfill composite cover systems. Computers and Geotechnics, 101, 80-94. https://doi.org/10.1016/j.compgeo.2018.04.021

Xie, H., Zuo, X., Yan, H., Peng, Y., Gu, X., Chen, Y., & Chen, Y. (2022). A steady-state analytical model for coupled methane transport and oxidation in vegetated landfill cover soil. Computers and Geotechnics, 152, 105006. https://doi.org/10.1016/j.compgeo.2022.105006

Xu, L., Lin, X., Amen, J., Welding, K., & McDermitt, D. (2014). Impact of changes in barometric pressure on landfill methane emission. Global Biogeochemical Cycles, 28(7), 679-695. https://doi.org/10.1002/2013GB004571

738 Xu, L., Ye, W. M., & Ye, B. (2017). Gas breakthrough in saturated compacted GaoMiaoZi (GMZ)
739 bentonite under rigid boundary conditions. Canadian Geotechnical Journal, 54(8), 1139-1149.
740 https://doi.org/10.1139/cgj-2016-0220

741 Yao, X. Z., Ma, R. C., Li, H. J., Wang, C., Zhang, C., Yin, S. S., Wu, D., He, X. Y., Wang, J.,
742 Zhan, L. T., & He, R. (2019). Assessment of the major odor contributors and health risks of volatile
743 compounds in three disposal technologies for municipal solid waste. Waste Management, 91, 128-
744 138. https://doi.org/10.1016/j.wasman.2019.05.009

745 Yan, H., Sedighi, M. & Jivkov, A.P. (2020). Peridynamics modelling of coupled water flow and
746 chemical transport in unsaturated porous media. Journal of Hydrology, 591, p.125648.
747 https://doi.org/10.1016/j.jhydrol.2020.125648

748 Yan, H., Jivkov, A. P., & Sedighi, M. (2022). Modelling soil desiccation cracking by
749 peridynamics. Géotechnique, 1-13. https://doi.org/10.1680/jgeot.21.00032

750 Zhan, L. T., Xu, H., Chen, Y. M., Lü, F., Lan, J. W., Shao, L. M., Lin, W. A., & He, P. J. (2017).
751 Biochemical, hydrological and mechanical behaviors of high food waste content MSW landfill:
752 Preliminary findings from a large-scale experiment. Waste Management, 63, 27-40.
753 https://doi.org/10.1016/j.wasman.2017.03.008

754 Zhan, T. L., Xu, X. B., Chen, Y. M., Ma, X. F., & Lan, J. W. (2015). Dependence of gas collection
755 efficiency on leachate level at wet municipal solid waste landfills and its improvement methods in
756 China. Journal of Geotechnical and Geoenvironmental Engineering, 141(4), 04015002.
757 https://doi.org/10.1061/(ASCE)GT.1943-5606.0001271
758

Table list

763 **Table 1.** The ranges of atmospheric conditions during the field test

Dates	Temperature (℃)	Wind speed (m/s)	Air humidity (%)
22nd May	20-32	0.3-3.2	50-90
25th June	24-38	0.3-4.1	40-95

764
765

766
767 **Table 2.** Parameters for benzene and dichloromethane.

	K_H	$\triangle H_{aw}$ (kJ/mol)	D_{g0} (m^2/s)	D_{w0} (m^2/s)	K_{oc0}	$\triangle H_{sorp}$ (kJ/mol)	μ (Pa*s)
benzene	0.214[b]	30[a]	8.9×10^{-6}[b]	1.03×10^{-9}[b]	66[c]	-9.61[g]	6.128×10^{-4}[b]
dichloromethane (DCM)	0.0994[b]	35[a]	1.05×10^{-5}[b]	1.23×10^{-9}[b]	114.8[d]	-48.6[f]	4.13×10^{-4}[b]

768 T_0 =25℃, R=8.314
769 [a] Schwarzenbach et al. (2003)
770 [b] US EPA (2013)
771 [c] US EPA (1996)
772 [d] Delle (2001)
773 [e] Wang and Grathwohl (2013)
774 [f] Pré et al. (2002)
775 [g] Chiou and Shoup (1985)

Figure list

(a)

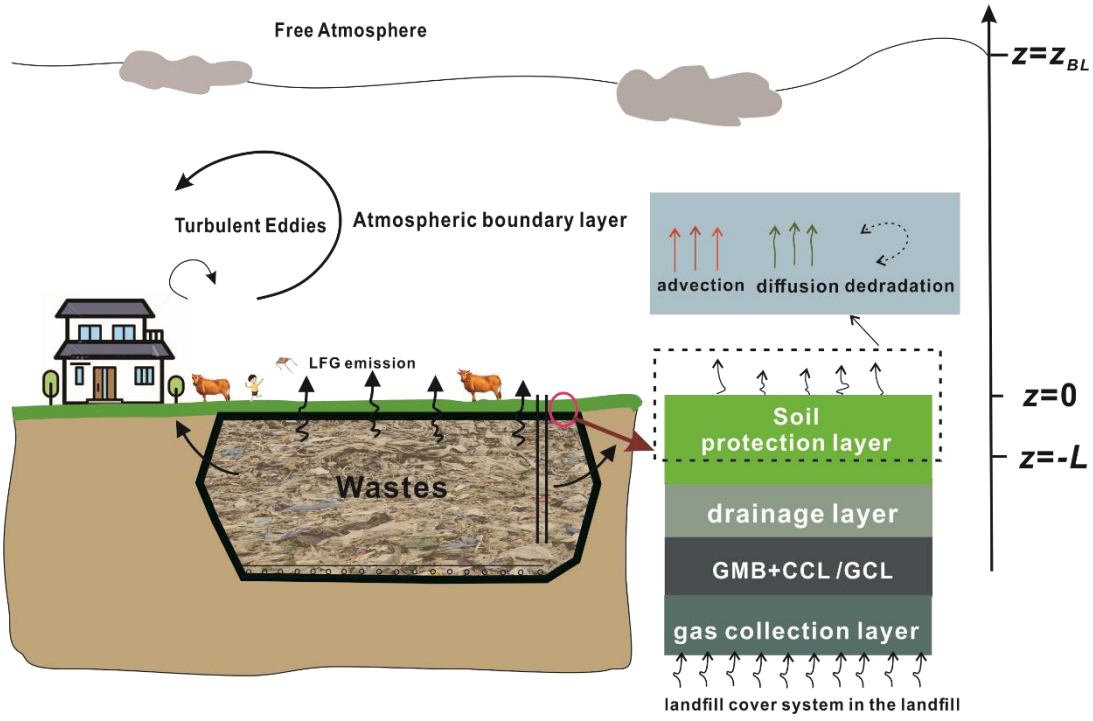

(b)

Figure 1. (a) The location of sampling points and (b)the conceptual model for VOCs transport and emission in a final landfill cover system.

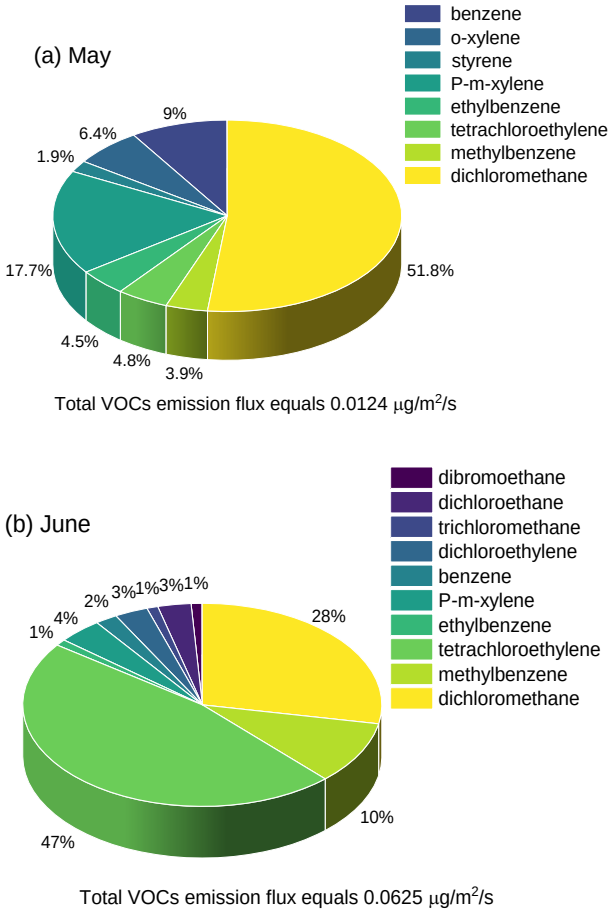

Figure 2. Emission flux and proportion of each VOCs in (a) May and (b) June.

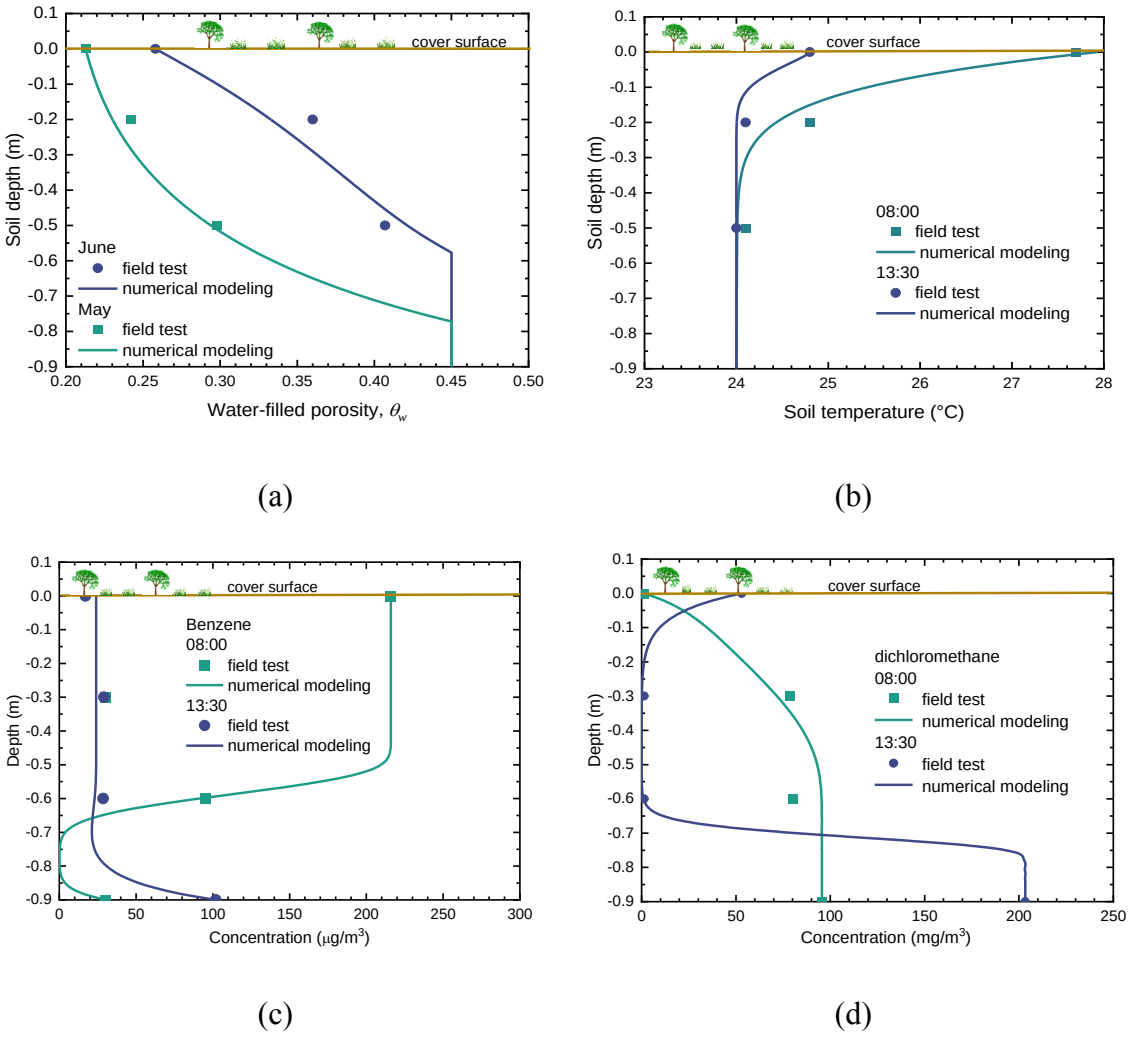

800 **Figure 3.** Validation of the proposed numerical model results with field test data for (a) soil
801 water content, (b) soil temperature, (c) benzene concentration profiles and (d) DCM
802 concentration profile.
803

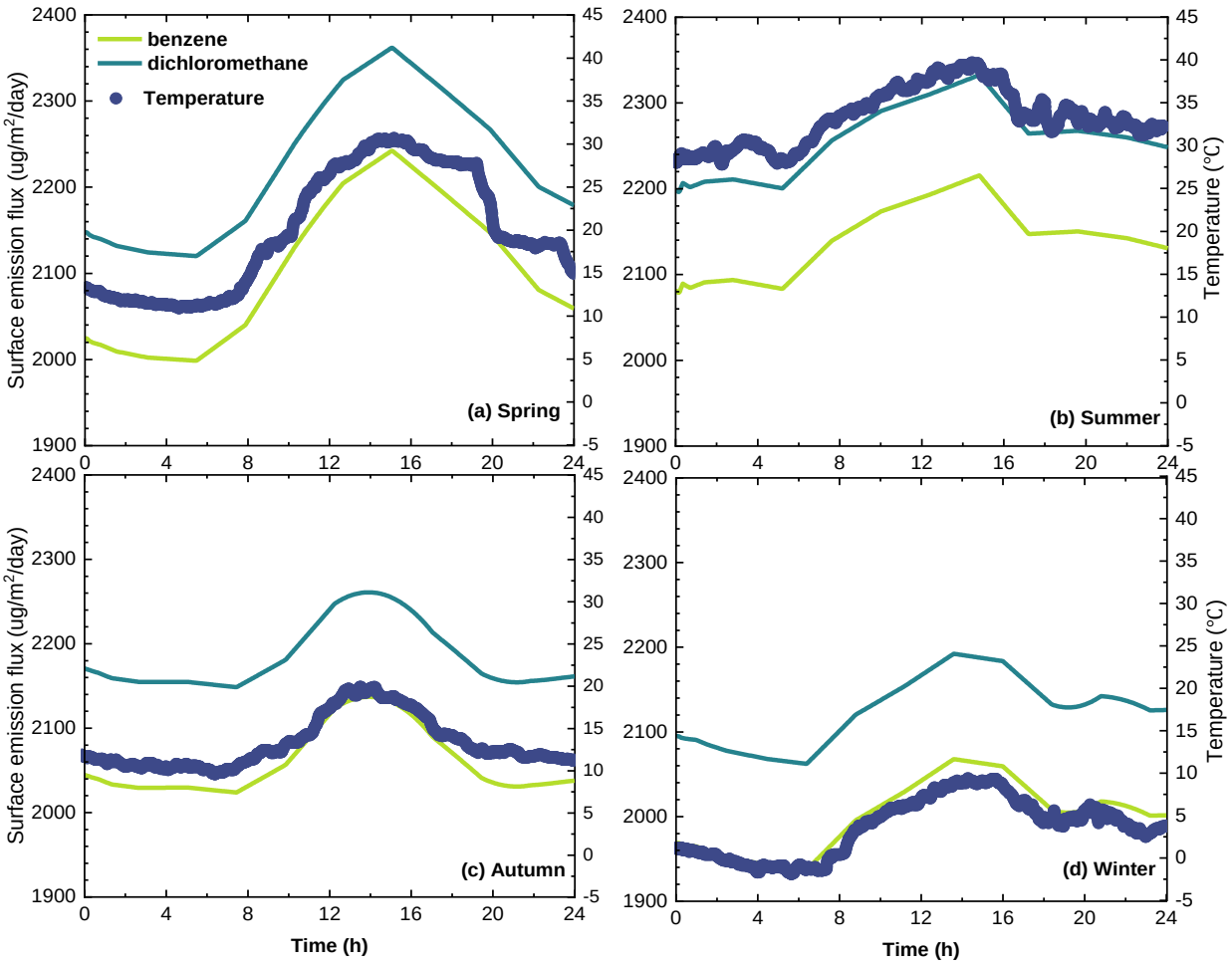

804

805

806 **Figure 4.** Estimated surface diffusive emission flux of benzene and DCM during a day in (a)

807 Spring, (b) Summer, (c) Autumn, and (d) Winter.

808

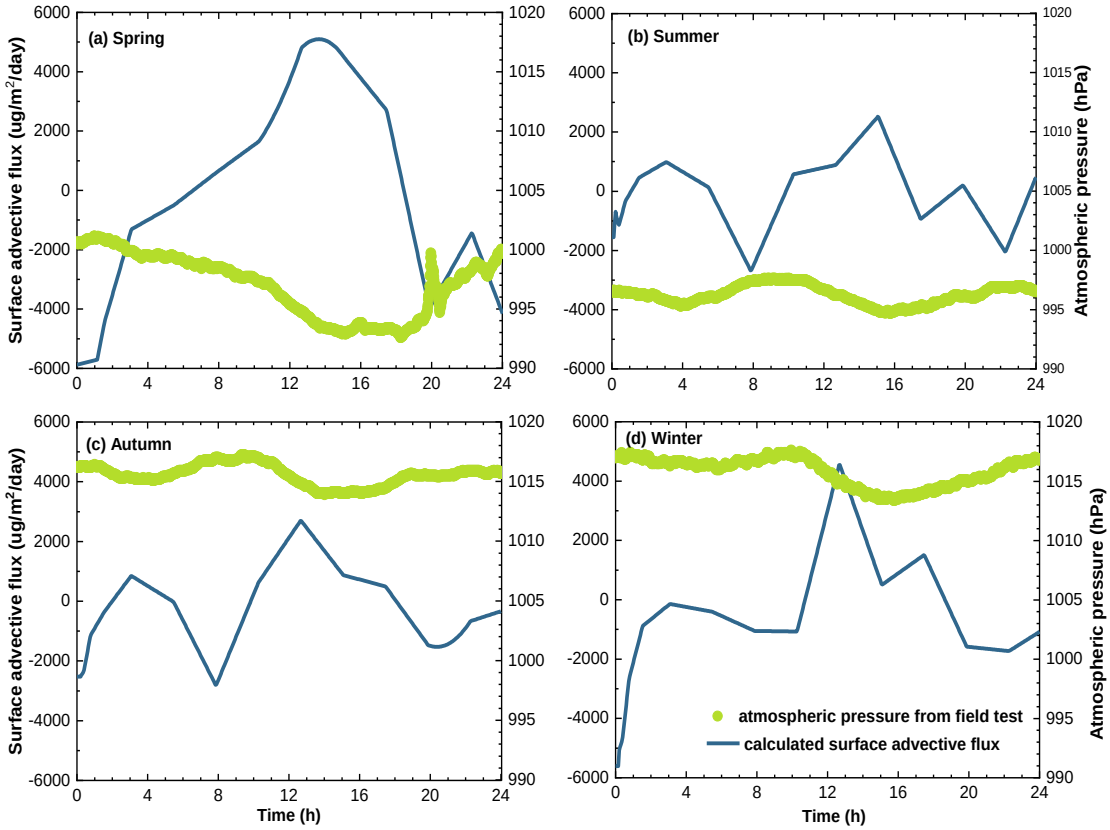

Figure 5. Estimated surface advective flux of benzene during a day in (a) Spring, (b) Summer, (c) Autumn, and (d) Winter.

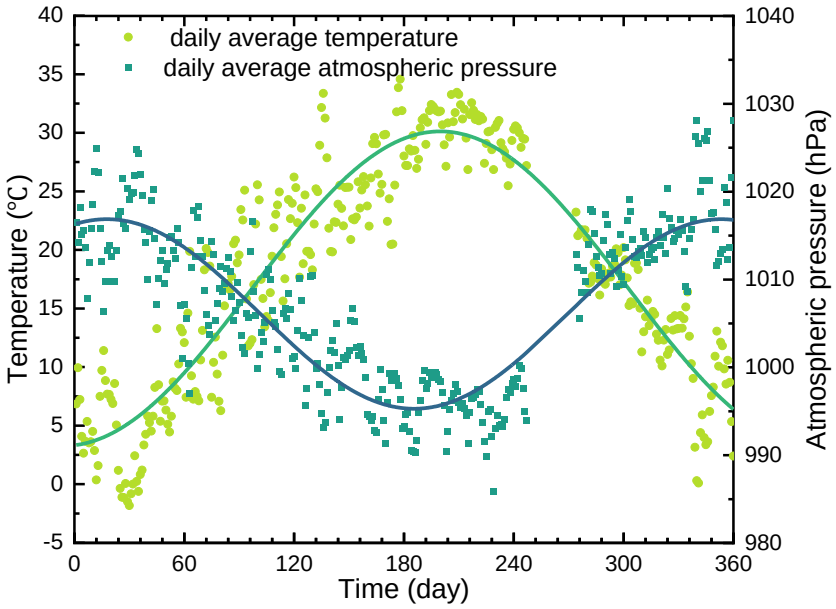

(a)

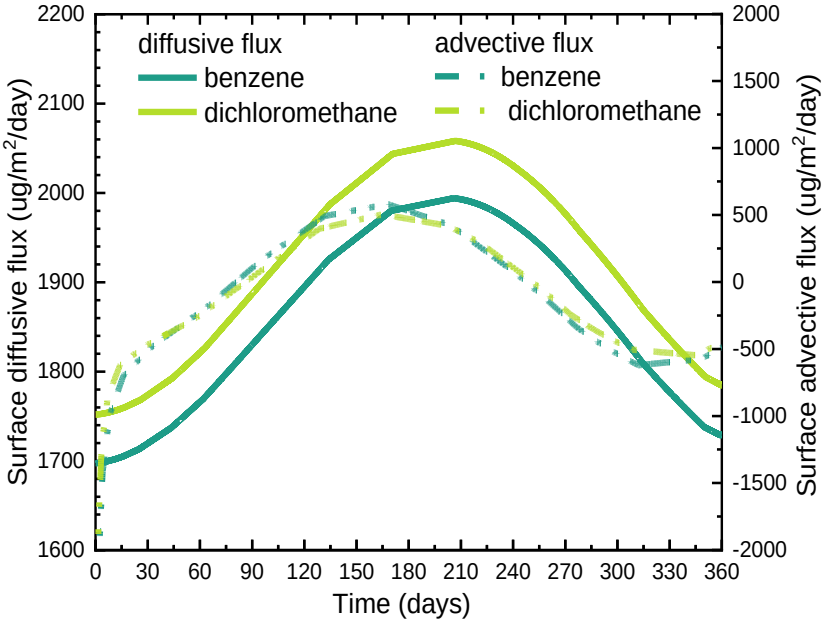

(b)

Figure 6. (a) Variation of temperature and pressure during the year by field test and (b) estimated VOC emission flux by numerical modeling.